Bond-impurity induced bound states in disordered spin-1/2 ladders

M. Arlego,[1,2] W. Brenig,[3] D. C. Cabra,[4] F. Heidrich-Meisner,[3] A. Honecker,[3,5] and G. Rossini[1,2]

[1] *Departamento de Física, Universidad Nacional de La Plata, C.C. 67, (1900) La Plata, Argentina*
[2] *Facultad de Ingeniería, Universidad de Lomas de Zamora, Camino de Cintura y Juan XXIII, (1832) Lomas de Zamora, Argentina*
[3] *Technische Universität Braunschweig, Institut für Theoretische Physik, Mendelssohnstrasse 3, 38106 Braunschweig, Germany*
[4] *Université Louis Pasteur, Laboratoire de Physique Théorique, 3 Rue de l'Université, 67084 Strasbourg Cedex, France*
[5] *Universität Hannover, Institut für Theoretische Physik, Appelstrasse 2, 30167 Hannover, Germany*

(Dated: May 11, 2004)

We discuss the effect of weak bond-disorder in two-leg spin ladders on the dispersion relation of the elementary triplet excitations with a particular focus on the appearance of bound states in the spin gap. Both the cases of modified exchange couplings on the rungs and the legs of the ladder are analyzed. Based on a projection on the single-triplet subspace, the single-impurity and small cluster problems are treated analytically in the strong-coupling limit. Numerically, we study the problem of a single impurity in a spin ladder by exact diagonalization to obtain the low lying excitations. At finite concentrations and to leading order in the inter-rung coupling, we compare the spectra obtained from numerical diagonalization of large systems within the single-triplet subspace with the results of diagrammatic techniques, namely low-concentration and coherent-potential approximations. The contribution of small impurity clusters to the density of states is also discussed.

I. INTRODUCTION

Since the synthesis of spin ladder materials such as $SrCu_2O_3$ (Ref. 1) or $(Sr,Ca,La)_{14}Cu_{24}O_{41}$ (Ref. 2) and the later discovery of superconductivity under high pressure in $Sr_{0.4}Ca_{13.6}Cu_{24}O_{41.84}$ (Ref. 3), spin-1/2 two-leg spin ladders have been on the focus of theoretical activities (see Refs. 4 and 5 for review). This model is of particular interest, as the ground-state is nonmagnetic and it is an example for a spin liquid. Many properties of the pure system, such as the dispersion of elementary excitations[6,7,8,9] and the thermodynamics[10] are well understood. The elementary excitations are propagating, massive triplet-modes.

A natural extension of the pure spin model comprises the inclusion of impurities. In this paper, we discuss the effect of impurities on the dispersion relation of the elementary triplet excitations and focus on the appearance of bound states in the spin gap. Such states could be visible in resonant experiments. One may distinguish between different kinds of impurities. First, magnetic ions, such as the Cu^{2+} ions in $SrCu_2O_3$, can be replaced by nonmagnetic ones such as Zn (see Ref. 11 and references therein), effectively removing a spin-1/2 moment, or by other ions with the same or a different effective moment. The replacement of the spin-carrying ion will be referred to as a site impurity. Note that it is also conceivable that a site impurity leads to modifications of the exchange couplings to neighboring sites. Second, and this is what we mainly have in mind in this study, the exchange paths themselves can be modified by doping the bridging X-ions in, e.g., Cu-X-Cu bonds, realizing what we call a bond impurity (or simply impurity) in the following. Such a situation is described in Ref. 12 for the alternating spin chain system $(CH_3)_2CHNH_3Cu(Cl_xBr_{1-x})_3$ where Cl and Br ions are substituted with each other. Furthermore, a spin ladder material exists, namely $(C_5H_{12}N)_2CuBr_4$ (Ref. 13) where one could think of analogous doping experiments. This material is suggested to contain two-leg spin ladders in the strong-coupling limit, i.e., the coupling constant along the legs J_L is small compared to the coupling along the rungs J_R; see Ref. 13. Moreover, there are a number of further candidates for organic spin ladder materials in the strong-coupling limit, see, e.g., Ref. 14. As an example for an inorganic system, we mention CaV_2O_5 for which a ratio of $J_\mathrm{L}/J_\mathrm{R} \sim 0.1$ is discussed[15].

In the literature, bond randomness in spin ladder systems has been studied both in the weak and strong disorder limit using the real-space renormalization group method[16,17], bosonization[18], and a mapping on random-mass Dirac fermions[19]. Most of these studies have focused on the stability of the ground state and the gap against disorder and they find that disordered spin ladders exhibit nonuniversal thermodynamic properties (see, e.g., Ref. 17) similar to disordered dimerized spin-1/2 chains[20].

The plan of the paper is the following. First, we introduce the model and perform a projection on the one triplet subspace in Sec. II. This approximation provides results which are correct in leading order of the inter-rung coupling and are quantitatively relevant for spin ladder materials in the strong-coupling limit. Second, the single-impurity problem is solved analytically in Sec. III in the strong-coupling limit. Also, we analyze small clusters of bond impurities on neighboring bonds. The results, i.e., the eigenenergies of single-impurity (anti-) bound states are then compared to those of a Lanczos study for the full spin ladder model. In Sec. IV, finite concentrations of bond-impurities are considered in the strong-

coupling limit. This problem is tackled both numerically and analytically by means of diagrammatic approaches [low-concentration approximation and coherent-potential approximation (CPA)]. The comparison of the numerical results with the analytical approaches provides insight into the validity of the latter methods. Finally, our conclusions are summarized in Sec. V

II. MODEL

The Hamiltonian of the pure two-leg spin ladder reads

$$H_0 = \sum_{l=1}^{N} [J_{\rm R} \vec{S}_{l,1} \cdot \vec{S}_{l,2} + J_{\rm L} (\vec{S}_{l,1} \cdot \vec{S}_{l+1,1} + \vec{S}_{l,2} \cdot \vec{S}_{l+1,2})]. \quad (1)$$

$\vec{S}_{l,1(2)}$ are spin-1/2 operators acting on site l on leg 1(2) and N is the number of rungs. For the remainder of the paper, we set $J_{\rm R} = 1$ in all explicit computations, but we keep $J_{\rm R}$ in the equations for clarity. We will discuss the following situations

$$H = H_0 + H'; \quad H' = \sum_{n=1}^{N_{\rm imp}} h_n \quad (2)$$

where $N_{\rm imp}$ is the number of modified couplings and h_n is the local perturbation at site l_n leading to either a modified on-site rung interaction $J'_{\rm R} = J_{\rm R} + \delta J_{\rm R}$ or a modified leg coupling $J'_{\rm L} = J_{\rm L} + \delta J_{\rm L}$, connecting sites l_n and $l_n + 1$. Explicitly, h_n reads

$$h_n = \delta J_{\rm R} \, \vec{S}_{l_n,1} \cdot \vec{S}_{l_n,2} \quad (3)$$

$$h_n = \delta J_{\rm L} \, \vec{S}_{l_n,j} \cdot \vec{S}_{l_{n+1},j}; \quad j = 1, 2. \quad (4)$$

The effect of modified interactions on the one-triplet dispersion will be discussed in the strong-coupling limit $J_{\rm L} \ll J_{\rm R}$ by projecting on the one-triplet subspace. Therefore, all terms contained in H_0 destroying or creating two triplet excitations are neglected. For the latter application of diagrammatic techniques, it is useful to map the spin operators on so called bond-operators[21,22] $s_l^{(\dagger)}, t_{\alpha,l}^{(\dagger)}$; $\alpha = x, y, z$. $s_l^\dagger$ creates a singlet on the lth rung out of the vacuum state $|\,0\rangle$ and $t_{\alpha,l}^\dagger$ creates a triplet excitation with orientation α, respectively. The exact representation of $S_{l,1(2)}^\alpha$, $\alpha = x, y, z$, in terms of bond-operators reads[22]

$$S_{l,j}^\alpha = (1/2)\{\pm s_l^\dagger t_{\alpha,l} \pm t_{\alpha,l}^\dagger s_l - i\epsilon_{\alpha\beta\gamma} t_{\beta,l}^\dagger t_{\gamma,l}\}. \quad (5)$$

The plus sign corresponds to $j = 1$ and the minus sign to $j = 2$; j labeling the leg. To avoid unphysical double occupancies one has to impose the local constraint (summation over repeated indices is implied in the following)

$$s_l^\dagger s_l + t_{\alpha,l}^\dagger t_{\alpha,l} = 1. \quad (6)$$

Projecting on the one-triplet subspace and thereby applying a Holstein-Primakoff type of approximation[21,23] $s_l = s_l^\dagger \approx 1$ results in the effective Hamiltonian

$$H_{0,\rm eff} = J_{\rm R} \sum_l t_{\alpha,l}^\dagger t_{\alpha,l} + \frac{J_{\rm L}}{2} \sum_l (t_{\alpha,l+1}^\dagger t_{\alpha,l} + \text{H.c.}) \quad (7)$$

where we have dropped irrelevant additive constants. $H_{0,\rm eff}$ is diagonalized by a Fourier transformation $t_{\alpha,l}^\dagger = (1/\sqrt{N}) \sum_k e^{-ikl} t_{\alpha,l}^\dagger$ leading to

$$H_{0,\rm eff} = \sum_k \epsilon_k t_{\alpha,k}^\dagger t_{\alpha,k} \quad (8)$$

and the dispersion relation of one-triplet excitations is[6]

$$\epsilon_k = J_{\rm R} + J_{\rm L} \cos(k). \quad (9)$$

The perturbations h_n caused by modifications of the exchange couplings are expressed in terms of bond-operators as follows

$$h_n = \frac{1}{N} \sum_{k,k_1} v_{\rm R(L)}(k, k_1) \, t_{\alpha,k}^\dagger t_{\alpha,k_1} \quad (10)$$

with the potentials $v_{\rm R(L)}(k, k_1)$ given by

$$v_{\rm R}(k, k_1) = \delta J_{\rm R} \, e^{i l_n \Delta k} \quad (11)$$

$$v_{\rm L}(k, k_1) = \frac{\delta J_{\rm L}}{4} (e^{i l_n \Delta k} e^{i k_1} + e^{-i l_n \Delta k} e^{-ik}) \quad (12)$$

where $\Delta k = k_1 - k$ is the momentum transferred in a scattering process. All together, the effective Hamiltonian takes the form

$$H_{\rm eff} = H_{0,\rm eff} + H'_{\rm eff}; \quad H'_{\rm eff} = \sum_{n=1}^{N_{\rm imp}} h_n. \quad (13)$$

III. THE SINGLE-IMPURITY PROBLEM AND SMALL IMPURITY CLUSTERS

The solution of the one-impurity problem for the effective Hamiltonian Eq. (13), i.e., one modified coupling, is derived from Schrödinger's equation in real space. Here, we briefly outline the procedure and our results, referring the reader to the literature[24] for details. In addition, small impurity clusters are addressed and we study the problem of one impurity in the full model Eq. (2) using the Lanczos method.

A. Single-impurity problem in real space

Schrödinger's equation can be cast in the form

$$\left[I - G^0(E) \, H'_{\rm eff}\right] |\,\psi\rangle = 0, \quad (14)$$

where $G^0(E) = (E - H_{0,\mathrm{eff}})^{-1}$ is the free Green's function operator associated to the effective one-particle Hamiltonian $H_{0,\mathrm{eff}}$ in Eq. (7) and $|\,\psi\rangle$ is an eigenstate of the Hamiltonian H_{eff}. A real-space representation can be given using the one-triplet basis $t_{\alpha,l}$, where matrix elements of $G^0(E)$ are diagonal in α and depend only on the distance $\Delta l = |l - l'|$. In the continuum limit $N \to \infty$, they are given by

$$\left[G^0(E)\right]_{\Delta l}^{\alpha,\beta} = \delta_{\alpha\beta} \frac{1}{2\pi} \int_{-\pi}^{\pi} \frac{\cos(k\Delta l)}{E - J_R - J_L \cos\ k}\, dk\ , \quad (15)$$

with $\alpha, \beta = x, y, z$. Although E needs to be analytically continued to the complex plane in order to obtain the retarded Green's function by setting $E \to E + i0^+$, notice that for real E, $|E - J_{\mathrm{R}}| > J_{\mathrm{L}}$, matrix elements in Eq. (15) are real. For simplicity, we place the modified rung-coupling on site $l = 0$ and the modified leg-coupling between sites $l = 0$ and $l = 1$. The (anti-) bound states are found by setting the determinant of $I - G^0(E)\, H'_{\mathrm{eff}}$ to zero, and, due to the impurity location, at most the upper 2×2 submatrix needs to be considered. Notice, however, that the eigenvalues are threefold degenerate because of the three triplet modes $\alpha = x, y, z$.

The eigenenergy of the (anti-) bound state in the single rung-impurity case $\delta J_R \neq 0, \delta J_L = 0$ is obtained as

$$E_{1,\mathrm{R}} = J_{\mathrm{R}} \pm \sqrt{J_{\mathrm{L}}^2 + (\delta J_{\mathrm{R}})^2}; \quad \delta J_{\mathrm{R}} \gtrless 0. \quad (16)$$

The plus(minus) sign in Eq. (16) corresponds to $\delta J_{\mathrm{R}} > 0$ ($\delta J_{\mathrm{R}} < 0$). Therefore, a bound state in the spin gap, i.e., below the original one-triplet band, appears for $\delta J_{\mathrm{R}} < 0$. Conversely, for $\delta J_{\mathrm{R}} > 0$, there is an anti-bound state above the one-triplet band.

Analogously, one finds the eigenenergies of (anti-) bound states in the single leg-impurity case for $\delta J_R = 0, \delta J_L \neq 0$. For $\delta J_{\mathrm{L}} > 0$, there are always both a bound and an anti-bound state, their energies given by

$$E_{1,\mathrm{L}} = J_{\mathrm{R}} \pm \frac{J_{\mathrm{L}} + \frac{\delta J_{\mathrm{L}}}{2}(1 + \frac{\delta J_{\mathrm{L}}}{4J_{\mathrm{L}}})}{1 + \frac{\delta J_{\mathrm{L}}}{2J_{\mathrm{L}}}}; \quad \delta J_{\mathrm{L}} > 0. \quad (17)$$

On the other hand, we note that there are no states outside the one-triplet band for $-4J_{\mathrm{L}} < \delta J_{\mathrm{L}} < 0$; instead, we expect the appearance of resonant modes inside the band [see Sec. IV B, Fig. 5 (c)]. Finally, for strong ferromagnetic coupling $\delta J_L < -4J_L$, Eq. (17) again has two solutions; however, we will restrict the discussion to the case of antiferromagnetic couplings.

The wave function for (anti-) bound states $\psi_\alpha(l)$ can also be derived in a closed form:

$$\begin{aligned} &\delta J_{\mathrm{R}} \neq 0\ ;\ \delta J_{\mathrm{L}} = 0: \\ &\qquad \psi_\alpha(l) \propto [G^0(E_{1,\mathrm{R}})]_l^{\alpha\alpha} \quad (l > 0), \quad (18) \\ &\delta J_{\mathrm{R}} = 0\ ;\ \delta J_{\mathrm{L}} \neq 0: \\ &\qquad \psi_\alpha(l) \propto [G^0(E_{1,\mathrm{L}})]_l^{\alpha\alpha} + [G^0(E_{1,\mathrm{L}})]_{l-1}^{\alpha\alpha} \\ &\qquad\quad (l > 1). \quad (19) \end{aligned}$$

The width of $\psi_\alpha(l)$ in real space only depends on the ratio of $\delta J_{\mathrm{R}}/J_{\mathrm{L}}$ (or $\delta J_{\mathrm{L}}/J_{\mathrm{L}}$, respectively). The spatial extent of $|\psi_\alpha(l)|^2$ is the narrower, the larger this ratio is. For instance, $|\psi_\alpha(l = 4)|^2/|\psi_\alpha(l = 1)|^2 < 0.01$ for $\delta J_{\mathrm{R}}/J_{\mathrm{L}} = 1, \delta J_{\mathrm{L}} = 0$, while $|\psi_\alpha(l = 4)|^2/|\psi_\alpha(l = 1)|^2 \sim 0.15$ for $\delta J_{\mathrm{R}}/J_{\mathrm{L}} = 1/3$.

B. Impurity clusters

Solving Schrödinger's equation Eq. (14) in real space allows for the discussion of small impurity clusters. We consider the presence of impurities of the same type located on some of the first N_c ladder sites. The (anti-) bound eigenenergies depend in principle on both the number of modified couplings and their distance as well as the perturbation $\delta J_{\mathrm{R[L]}}$ itself. It is natural to expect the one-impurity eigenstates to interfere when the single impurities come close enough.

As before, the eigenenergies of the cluster are evaluated by setting the determinant of $I - G^0\,(E)\ H'_{\mathrm{eff}}$ to zero. Now, only the upper $N_c \times N_c$ submatrix needs to be considered. As an example, we give the analytical expression for the case of two modified rung couplings on neighboring sites ($N_c = 2$). One solution exists for both $\delta J_{\mathrm{R}} < 0$ (inside the gap) or $\delta J_{\mathrm{R}} > 0$ (above the one-triplet band). Their eigenenergies $E_{2,\mathrm{R}}$ read

$$E_{2,\mathrm{R}} = \frac{J_{\mathrm{L}} J_{\mathrm{R}} \pm J_{\mathrm{L}}^2 + 2J_{\mathrm{L}}\delta J_{\mathrm{R}} \pm 2\delta J_{\mathrm{R}}(J_{\mathrm{R}} + \delta J_{\mathrm{R}})}{J_{\mathrm{L}} \pm 2\delta J_{\mathrm{R}}}\,. \quad (20)$$

The plus sign has to be used for $\delta J_{\mathrm{R}} > 0$ and the minus sign in the opposite case. We have computed similar expressions for clusters up to $N_c = 5$. In Sec. IV C, we will show that the influence of such clusters explains the details of the peak structure in the density of states obtained by numerical diagonalization of systems with a finite impurity concentration.

C. Comparison with exact diagonalization

To test the region of validity of the results derived above to first order in $J_{\mathrm{L}}/J_{\mathrm{R}}$, we now compare them to numerical results for the full spin ladder Hamiltonian Eq. (2) with one modified rung or leg coupling.

We have exploited S^z-conservation, spin-inversion symmetry, reflection symmetry at the impurity bond and, in the case of a rung impurity, exchange symmetry of both legs. Usually, one uses periodic boundary conditions and exploits translational invariance. Although the latter is not possible if an impurity is present, we still apply periodic boundary conditions along the legs in order to minimize surface effects. Finite-size effects turn out to be smallest for an even number of rungs. We therefore concentrate on systems with $N = 4$, 6, 8, 10, 12, and 14 rungs. The largest dimension is slightly above 10 million and occurs for $N = 14$ rungs (28 spins) and

one leg impurity (where exchange symmetry of the legs is absent).

In each of the relevant subspaces we have computed the lowest eigenvalue using the Lanczos procedure. The results for the lowest excitation energy E at finite N have then been extrapolated to the thermodynamic limit $N \to \infty$ using the Vanden-Broeck-Schwartz-algorithm[25,26] with $\alpha = -1$. For the pure ladder this yields estimates for the spin gap shown by the open circles in Fig. 1. Using $N \leq 14$, we find a value of $(0.5025 \pm 0.0008) J_{\rm R}$ at $J_{\rm L} = J_{\rm R}$, in excellent agreement with accepted values for this case (see section III.A of Ref. 10 for a summary). As a further comparison, the full line in Fig. 1 shows a [7,6] Padé approximant to the 13th order series for the spin gap of the pure ladder of Ref. 9.

A finite number of impurities (vanishing density) does not affect the one-triplet band in the thermodynamic limit. Hence, the result for the spin gap in the pure case also corresponds to the lower boundary of the one-triplet band if impurities are present.

Turning now to the case of *one* impurity, we concentrate on those situations where we may expect the lowest excitation to be a bound state at the impurity, namely $\delta J_{\rm R} < 0$ or $\delta J_{\rm L} > 0$, respectively. To understand the finite-size behavior of systems with one impurity, it is important to realize that there are now two competing length scales involved. On the one hand, there is the correlation length of the pure system, and on the other hand, the spatial extent of the impurity wave function needs to be considered [see Eqs. (18) and (19)]. Indeed, the typical width of the impurity wave function, which depends on the actual choice of parameters, can be (much) bigger than the correlation length. This interplay leads to a crossover in the finite-size behavior.

For small $J_{\rm L}$, the energy of the impurity level increases with system size which is in contrast to the behavior of the pure system where the energy of the lower edge of the band decreases with system size. Since the latter finite-size behavior is preserved at large $J_{\rm L}$, finite-size effects are nonmonotonic in the intermediate region, i.e., the finite-size behavior changes at a characteristic system size that increases as the impurity level approaches the one-triplet band. One now has to be more careful with the extrapolation, and we can use only those system sizes which are in the asymptotic regime for large N. Accordingly, Fig. 1 shows extrapolated data points for the impurity level only in a restricted region of $J_{\rm L}$. When the impurity level approaches the one-triplet band, error bars become large, making it difficult to decide whether this level merges into the band or approaches it only asymptotically. In any case, the numerical data demonstrate the presence of an impurity bound state in a wide parameter region.

In the limit of small $J_{\rm L} \ll J_{\rm R}$, we can compare to Eqs. (16) and (17), respectively. One indeed observes quantitative agreement for sufficient small $J_{\rm L}$, see Fig. 1 (a) and the inset of Fig. 1 (b). Note that due to the

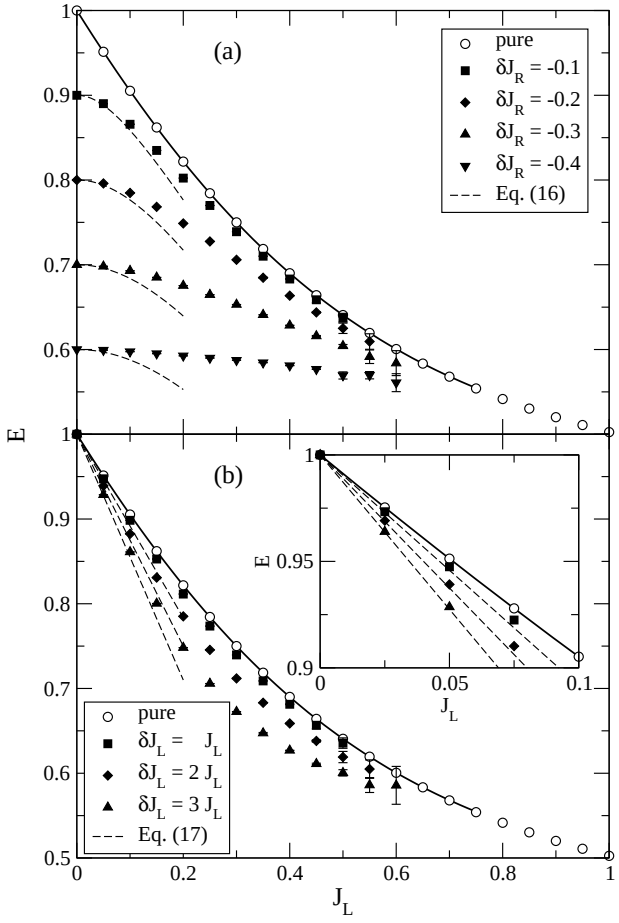

FIG. 1: Excitation energy E of the lowest level for the full spin ladder Hamiltonian (2). Panel (a): one rung impurity $J'_{\rm R} = J_{\rm R} + \delta J_{\rm R}$. Panel (b): one leg impurity $J'_{\rm L} = J_{\rm L} + \delta J_{\rm L}$. In all cases, the normalization is fixed to $J_{\rm R} = 1$. Symbols are obtained by extrapolation of Lanczos diagonalization on finite systems. Open circles are for the pure system ($\delta J_{\rm R} = 0$ and $\delta J_{\rm L} = 0$) and correspond to the spin gap; the solid line is a [7,6] Padé approximant to the 13th order strong-coupling series[9] for the spin gap of the pure ladder. Dashed lines display the analytical result for the position of the bound state in the effective Hamiltonian Eq. (13), namely Eq. (16) [panel (a)] and Eq. (17) [panel (b)].

normalization of Fig. 1, i.e., $\delta J_{\rm L} \sim J_{\rm L}$, Eq. (17) results in straight lines which start at $E = 1$ for $J_{\rm L} = 0$. At larger $J_{\rm L}$ deviations can be observed in Fig. 1, but an impurity level can still be seen. Accordingly, the first-order approximation can still be expected to be qualitatively correct even in a parameter region where it is no longer quantitatively accurate. Hence, we may use the first-order approximation to study several impurities and even finite densities which is no longer systematically possible by Lanczos diagonalization of the full ladder Hamiltonian.

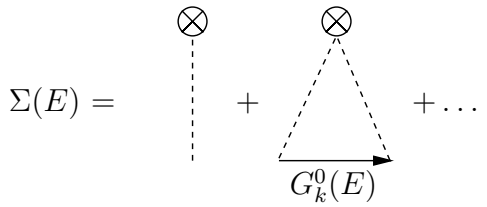

FIG. 2: Sketch of the diagrammatic expansion of the self energy $\Sigma(E)$ in the low-concentration limit. $G_k^0(E) = 1/(E - \epsilon_k)$ is the free one-triplet Green's function.

IV. FINITE CONCENTRATIONS

In this section, we discuss the effect of a finite concentration of modified couplings J_R or J_L on the one-triplet dispersion in the strong-coupling limit $J_\mathrm{L} \ll J_\mathrm{R}$. To treat this problem, we apply diagrammatic techniques, namely, a low-concentration approximation (LCA) and the coherent-potential approximation (CPA), and numerical diagonalization of large systems. We also use our analytical results for the eigenenergies of small impurity clusters to explain the details in the numerical results for the density of states, both for (anti-) bound states and resonance modes.

Before we turn to the discussion of the analytical methods and compare the results to those from numerical impurity averaging (NAV), let us consider certain limiting cases. In the following, c denotes the concentration of impurities. Note that in the case of impurities on the legs, we set $c = 1$ if all $2N$ couplings are modified.

The limiting cases are: (i) the pure system ($c = 0$); (ii) the single-impurity case (see Sec. III A); (iii) the case $c = 1$ where all couplings are equal to $J_\mathrm{R} + \delta J_\mathrm{R}$ or $J_\mathrm{L} + \delta J_\mathrm{L}$, respectively. In the latter case and for $\delta J_\mathrm{R} \neq 0, \delta J_\mathrm{L} = 0$, a one-triplet band with the dispersion $E_k = (J_R + \delta J_R) + J_\mathrm{L}\cos(k)$ will result, i.e., its center is shifted by δJ_R with respect to the center of the original band for $c = 0$. Therefore, the single-impurity (anti-) bound state should develop into a dispersive band as the concentration increases while the center $\epsilon(c)$ of the band lies between $J_\mathrm{R} - \sqrt{J_\mathrm{L}^2 + (\delta J_\mathrm{R})^2} < \epsilon(c) < J_\mathrm{R} + \delta J_\mathrm{R}$ for $\delta J_\mathrm{R} < 0$. An analogous scenario arises for $\delta J_\mathrm{R} > 0$.

For $\delta J_\mathrm{R} = 0, \delta J_\mathrm{L} > 0$, the triplet dispersion in the limit of $c = 1$, i.e., all J_L modified, reads $E_k = J_\mathrm{R} + (J_\mathrm{L} + \delta J_\mathrm{L})\cos(k)$. Thus, the bound- and anti-bound states appear symmetrically with respect to the center of the original band. On increasing the concentration c, additional impurity levels will appear and eventually, they will merge in the original band. Finally, there will be one broadened band possessing a bandwidth of $(J_\mathrm{L} + \delta J_\mathrm{L})$.

A. Low-concentration and coherent-potential approximation

Based on a diagrammatic expansion of the one-triplet Green's function in the presence of impurities, a number of useful methods exist to get approximate results for the self-energy $\Sigma(E)$. First, we briefly comment on the low-concentration approximation and second, we discuss results from the coherent-potential approximation.

As in Sec. III we will concentrate on the single-triplet subspace. Thus, apart from integrating out the singlet, the hard-core constraint Eq. (6) is automatically satisfied within our approximation, i.e., first-order perturbation theory in $J_\mathrm{L}/J_\mathrm{R}$.

Low-concentration approximation - Using standard impurity-averaging techniques (see, e.g., Ref. 27), the self-energy of the one-triplet Green's function can be obtained in first order in the impurity concentration. As the averaging procedure restores translational invariance, the one-triplet Green's function $G_k(E)$ can be written in terms of the Dyson equation

$$G_k(E) = \frac{1}{E - \epsilon_k - c\Sigma(E)}\,. \tag{21}$$

Keeping only terms linear in c implies that the self-energy $\Sigma(E)$ is equal to the $\hat{T}$-matrix of the one-impurity problem. The diagrammatic expansion of the self energy is sketched in Fig. 2. Note that all quantities in Eq. (21) become 2×2 matrices if the modified coupling connects two sites as realized by a leg impurity. For a more detailed discussion of this technique, the reader is referred to, e.g., Ref. 28.

The spectral function $A_k(E) = -(1/\pi)\mathrm{Im}G_k(E)$ is plotted in Fig. 3 for (a) $J_\mathrm{L} = 0.1, \delta J_\mathrm{R} = -0.1, c = 0.01$ and (b) for $J_\mathrm{L} = 0.1, \delta J_\mathrm{L} = 0.5, c = 0.01$. In accordance with our previous results we find one bound state in case (a) and a bound and an anti-bound state in case (b). Figure 3 further reveals that first, the impurity levels have developed a small dispersion and second, the spectral weight is concentrated around $k = \pi$ for the bound states while it vanishes in the center of the zone, and vice-versa for the anti-bound states.

Coherent-potential approximation - The coherent-potential approximation allows one to interpolate between the two limits of $c = 0$ and $c = 1$. Here, we apply this method to the case of $\delta J_\mathrm{R} < 0, \delta J_\mathrm{L} = 0$. The self-energy is obtained from a self-consistent solution of the equation[29]

$$\Sigma(E) = \frac{c\,\delta J_\mathrm{R}}{1 - G(E)\,[\delta J_\mathrm{R} - \Sigma(E)]}. \tag{22}$$

Rather than deriving this equation (see Ref. 29 for details), let us mention some features of this method: (i) the self-energy is symmetric under exchange of host and impurity sites, i.e., c and $1-c$ and the respective replacement of the coupling constants; and (ii) it gives qualitatively correct results for the density of states for intermediate concentrations. We note that in contrast to the low-concentration approximation [see, e.g., Fig. 4 (a)], the CPA does not lead to a sharp peak in the density

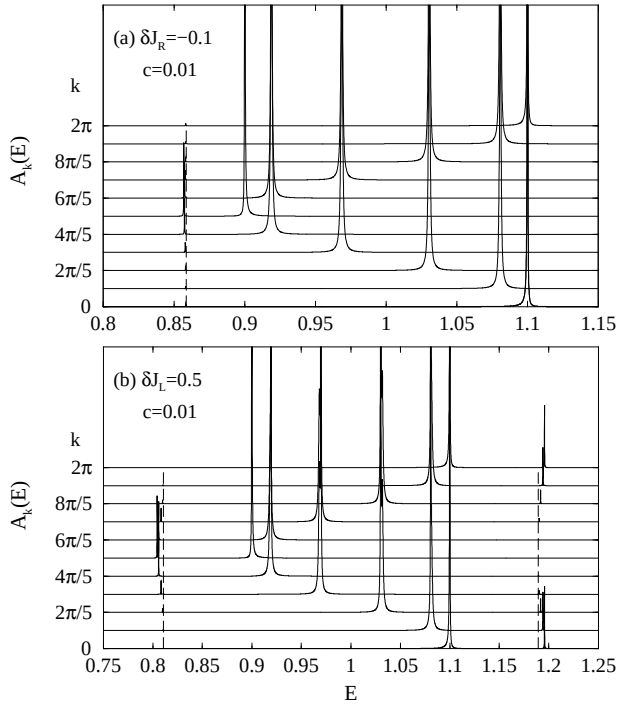

FIG. 3: Spectral function $A_k(E)$ in low-concentration approximation (LCA) for (a) perturbed rung couplings with $\delta J_{\rm R} = -0.1$, $c = 0.01$; (b) perturbed leg couplings with $\delta J_{\rm L} = 0.5$, $c = 0.01$. The dashed lines mark the positions of the (anti-) bound states from Eqs. (16) and (17). $J_{\rm R} = 1$ and $J_{\rm L} = 0.1$ in both cases.

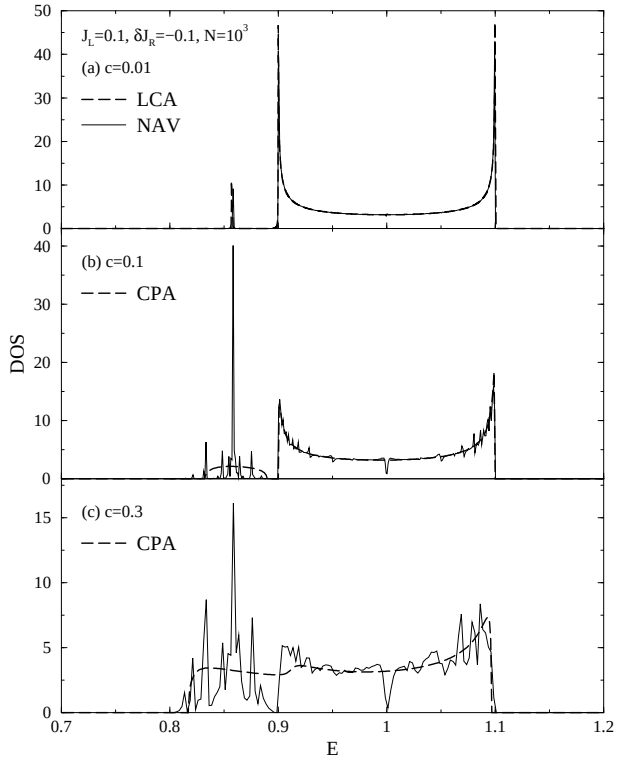

FIG. 4: Density of states (DOS) at finite concentration of modified couplings $J'_{\rm R}$: numerical data (NAV, solid line) for spin ladders with $N = 10^3$ rungs and $J_{\rm R} = 1, J_{\rm L} = 0.1, \delta J_{\rm R} = -0.1$ (concentration: panel (a) $c = 0.01$; panel (b) $c = 0.1$; panel (c) $c = 0.3$.). Dashed line in panel (a): low-concentration approximation (LCA); in panel (b) and (c): CPA.

of states at the position of the impurity level even for low concentrations. This can, for example, be seen in Fig. 4 (b) for $c = 0.1$. We have, however, checked that in both diagrammatic approaches, the total weight in the impurity levels is the same and that it grows linearly with the impurity concentration, as expected.

B. Numerical results and comparison

Now we compare the analytical results with a numerical diagonalization of the effective Hamiltonian on large systems and sampling over several realizations at fixed concentration. The effective Hamiltonian $H_{\rm eff}$ Eq. (13) has been diagonalized on finite systems with $N = 10^3$ rungs for different choices of impurity concentrations c for both types of bond impurities. The density of states (DOS) is obtained from binning the eigenvalues, the bin-width of typically $\Delta E \sim 10^{-3} J_{\rm R}$ determining the resolution in Figs. 4 to 7. Results are shown for $J_{\rm L} = 0.1, \delta J_{\rm R} = -0.1$ in Fig. 4 (panel (a): $c = 0.01$; (b): $c = 0.1$; (c): $c = 0.3$). Note that, according to Eq. (16), the position of the single-impurity level is $E_{1,{\rm R}} = 0.8586 J_{\rm R}$. The following features are observed: (i) for increasing concentration, additional peaks appear in the vicinity of the one-impurity level. They stem from impurity clusters, i.e., impurities occupying neighboring sites, as will be discussed in more detail below. (ii) The bound state level develops into a band centered around $J_{\rm R} + \delta J_{\rm R} = 0.9$ as a function of concentration c. Notice that larger concentrations $c > 0.5$ are conveniently realized by setting $c \to 1 - c, J_{\rm R} \to J_{\rm R} + \delta J_{\rm R}$, and $\delta J_{\rm R} \to -\delta J_{\rm R}$. (iii) Inside the original band, the curve is not smooth, but displays small oscillations. These features are neither due to finite-size effects nor due to low statistics (the density of states has been obtained by averaging over typically a few thousand random realizations at fixed concentration). As we shall discuss below, their origin can also be related to the effect of impurity clusters.

Let us now comment on the comparison of the numerical with the analytical results. By integrating $A_k(E)$ over the momentum k, the density of states $n(E)$ is obtained. Results from the LCA are compared to the numerical impurity averaging in the case of $J_{\rm L} = 0.1, \delta J_{\rm R} = -0.1, c = 0.01$ in Fig. 4 (a). Both approaches agree well with regard to the position of the main impurity level. The comparison with the results from the CPA for $c = 0.1$ [Fig. 4 (b)] and $c = 0.3$ [Fig. 4 (c)] shows that this approach gives qualitatively reasonable results even at fairly

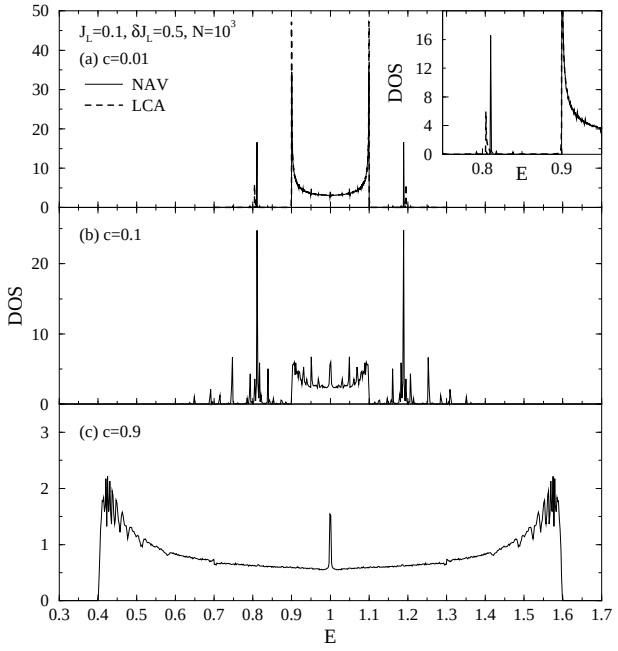

FIG. 5: Density of states (DOS) at finite concentration of modified couplings $J_{\rm L}'$: numerical data (NAV, solid line) for spin ladders with $N = 10^3$ rungs and $J_{\rm R} = 1, J_{\rm L} = 0.1$, and $\delta J_{\rm L} = 0.5$ (concentration: panel (a) $c = 0.01$; panel (b) $c = 0.1$; panel (c) $c = 0.9$.). Dashed line in panel (a): low-concentration approximation (LCA). Inset of panel (a): structure of the DOS in the vicinity of the bound state. Panel (c): one observes resonance modes inside the band for $c = 0.9$; the case shown here is equivalent to $J_{\rm L} = 0.6$, $\delta J_{\rm L} = -0.5 < 0$, and $c = 0.1$.

large concentrations. At $c = 0.3$, the impurity levels and the original band start to merge.

For a finite concentration of leg couplings, the numerical results confirm our qualitative expectations. The data are shown in Fig. 5 for $J_{\rm L} = 0.1, \delta J_{\rm L} = 0.5$ (panel (a): $c = 0.01$; (b): $c = 0.1$; (c): $c = 0.9$). For clarity, we note that the possible impurity configurations are: (i) one modified coupling on one leg, connecting, e.g., rung l and $l + 1$; and (ii) both couplings between rung l and $l + 1$ modified. Both cases are taken into account in the numerical implementation.

The impurity levels occur symmetrically with respect to the center of the band. On increasing the concentration c, the original band widens and eventually includes all impurity levels (see Fig. 5 (c) for $c = 0.9$). The influence of impurities is now visible as resonance modes inside the band. Note that the last case is equivalent to $J_{\rm L} = 0.6$, $\delta J_{\rm L} = -0.5$, and $c = 0.1$.

Comparing to the LCA from Eq. (21) for the case of $J_{\rm L} = 0.1, \delta J_{\rm L} = 0.5, c = 0.01$ [see Fig. 5 (a)], we see that the positions of the highest peaks seen in the numerical data and the analytical result almost coincide, similar to the case shown in Fig. 4 (a). The inset of Fig. 5 (a) contains a zoom of the region around the lower single-leg impurity peak with $E_{1,\rm L} = 0.811 J_{\rm R}$ revealing the presence of several less pronounced structures.

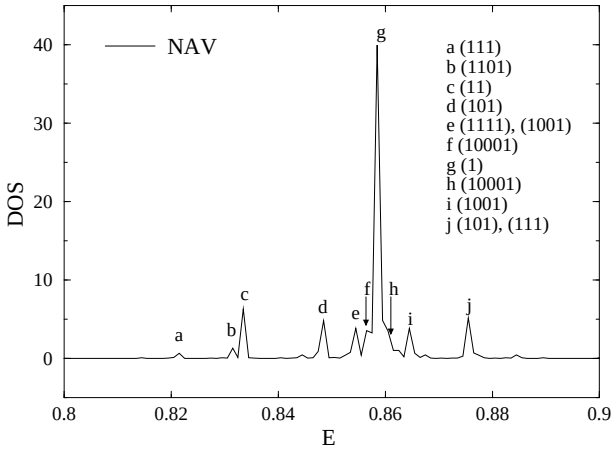

FIG. 6: Comparison of eigenenergies of bound states induced by rung-impurity clusters in a clean system, derived analytically, with numerical diagonalization of $H_{\rm eff}$ on large systems with a finite concentration of modified rung couplings. The density of states (DOS) in the vicinity of the one-impurity level is shown. The patterns in parenthesis denote different types of impurity clusters: with 1, we indicate the relative position of the rung impurities in the cluster sequence. The numerical data (NAV, solid line) correspond to $J_{\rm R} = 1, J_{\rm L} = 0.1$, $\delta J_{\rm R} = -0.1$ and $c = 0.1$. The letters 'a' to 'j' relate the peaks in the DOS to certain impurity clusters, which are listed in the legend.

In summary, the analytical approaches give fair results for the overall structure of the density of states even at large concentrations as exemplified in the case of $\delta J_{\rm R} < 0, \delta J_{\rm L} = 0$. The effects of impurity clusters are not taken into account in the diagrammatic description.

C. Analytical results for small impurity clusters

Next we analyze the details of the peak structure of the impurity levels arising from a variety of small impurity clusters for the case of modified rung couplings. The clusters analyzed include, e.g., the patterns (11), (101), (111), (1001), (1101), (1111), and (10001) where, in this notation, 1 indicates a modified rung in the cluster sequence and 0 indicates no impurity placed on a rung site. For example, (11) denotes two rung impurities on neighboring sites in an otherwise clean system.

We find that the energy eigenvalues corresponding to the main peaks outside the triplet band observed in the numerical results for the density of states (see the previous section) can be associated with the contribution of certain impurity clusters. In particular, in Fig. 6, we show the matching between the numerical bound state structure and the analytically computed eigenenergies corresponding to different small clusters placed in an otherwise clean system for the case of $J_{\rm L} = 0.1$, $\delta J_{\rm R} = -0.1$

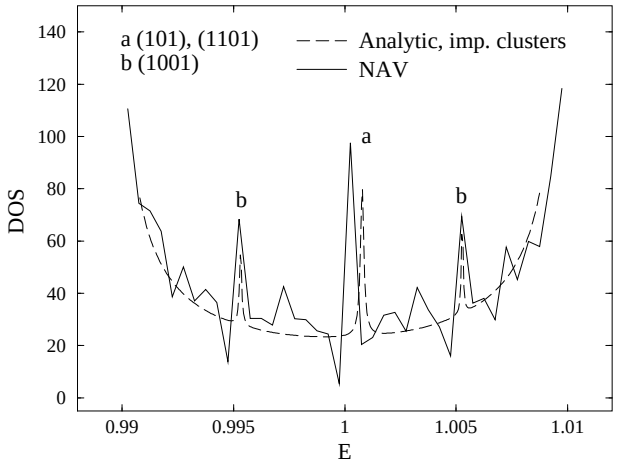

FIG. 7: Matching between the peak structure inside the triplet band obtained numerically at finite concentration of rung impurities (NAV, solid line) and analytically for systems with different types of impurity clusters (dashed line), for $J_{\rm R} = 1$, $J_{\rm L} = 0.01$, $\delta J_{\rm R} = -0.05$ and $c = 0.1$.

and $c = 0.1$ (see Fig. 4 (b) for the full density of states in the same case).

Let us now discuss the features inside the triplet band in the presence of impurities. The density of states (DOS) $n(E)$ can be evaluated from

$$n(E) = -\frac{1}{\pi}\mathrm{Im}\,\mathrm{Tr}\,G(E) = n_0(E) + n_{\rm imp}(E), \qquad (23)$$

where the free density of states[29] is $n_0(E) = -(1/\pi)\,\mathrm{Im}\,\mathrm{Tr}\,G^0(E)$ and the contribution from the impurities $n_{\rm imp}(E)$ can be written as

$$n_{\rm imp}(E) = -\frac{1}{\pi}\,\mathrm{Im}\frac{d}{dE}\ln\left[\mathrm{Det}\left(I - G^0\,(E)\;H'_{\rm eff}\right)\right]. \quad (24)$$

We use Eq. (24) to compute the contributions from particular impurity clusters to the DOS inside the triplet band. Moreover, from the amplitudes of the different peaks outside the one-triplet band, one can read off, at least qualitatively, the distribution of probabilities for the presence of the different clusters in a random sample of impurities for a given concentration. This information is in turn used to weight the influence of each cluster on the peak structure inside the triplet band. In Fig. 7, we show an example where the main peaks are associated with the corresponding cluster contributions. We are able to match, in this particular case, the central peak, which is slightly shifted to the right of the band-center, with the patterns (1101) and (101), and the two ones, which are almost symmetrical with respect to the band center, with a contribution from the (1001) cluster.

This analysis explains on the one hand the appearance of the various localized modes and on the other hand it gives evidence that the peaks inside the triplet band originate from the existence of impurity clusters.

V. DISCUSSION AND CONCLUSIONS

In this paper we have studied the appearance of bound states in the spin gap of spin ladders with bond impurities. Both the cases of modified rung and leg couplings have been considered. We have derived analytical results for the position of bound states in the strong-coupling limit equivalent to first order perturbation theory in $J_{\rm L}/J_{\rm R}$. The existence of impurity induced bound states has been verified by a Lanczos study of finite spin ladders with one impurity and $0 < J_{\rm L} \leq J_{\rm R}$ and we find that our analytical results are quantitatively correct for $J_{\rm L} \lesssim J_{\rm R}/10$ and that a qualitative agreement is still found for larger $J_{\rm L}$. Recently discovered spin ladder materials such as, for example, $(C_5H_{12}N)_2CuBr_4$ (Ref. 13) or CaV_2O_5 (Ref. 15) fall in this range of parameters.

Further, we have discussed the density of states in the presence of a finite concentration of impurities in the limit of $J_{\rm L} \ll J_{\rm R}$ both numerically and analytically. The comparison of the different approaches shows that diagrammatic methods give quantitatively correct results for small impurity concentrations and, furthermore, a qualitatively correct picture is obtained for large impurity concentrations. As the diagrammatic approaches neglect the interference of impurities and the effect of impurity clusters, we have presented a careful analysis of systems with small impurity clusters which allows us to understand details visible in the density of states. Natural extensions of this work, i.e., the computation of observables and the discussion of systems with arbitrary ratios of $J_{\rm L}/J_{\rm R}$, are left for future work. Nevertheless, our results already imply the appearance of additional features in the spin gap which could be observed by, e.g., optical experiments on bond-disordered spin ladder materials.

Acknowledgments - This work was supported by the DFG, Schwerpunktprogramm 1073, by a DAAD-ANTORCHAS exchange program, and by CONICET and Fundación Antorchas, Argentina. We acknowledge support by the Rechenzentrum of the TU Braunschweig where parts of the numerical computations have been performed on a COMPAQ ES45 (CFGAUSS).

[1] Z. Hiroi, M. Azuma, M. Takano, and Y. Bando, J. Solid State Chem. **95**, 230 (1991); M. Azuma, Z. Hiroi, M. Takano, K. Ishida, and Y. Kitaoka, Phys. Rev. Lett. **73**, 3463 (1994).

[2] E. M. Carron, M. A. Subramanian, J. C. Calabrese, and R. L. Harlow, Mater. Res. Bul. **23**, 1355 (1988).

[3] M. Uehara, T. Nagata, J. Akimitsu, H. Takahashi, N. Mori, and K. Kinoshita, J. Phys. Soc. Jpn. **65**, 2764 (1996).

[4] E. Dagotto and T. M. Rice, Science **271**, 618 (1996).
[5] E. Dagotto, Rep. Prog. Phys. **62**, 1525 (1999).
[6] T. Barnes, E. Dagotto, J. Riera, and E. S. Swanson, Phys. Rev. B **47**, 3196 (1993).
[7] M. Reigrotzki, H. Tsunetsugu, and T. M. Rice, J. Phys.: Condens. Matter **6**, 9235 (1994).
[8] M. Greven, R. J. Birgeneau, and U.-J. Wiese, Phys. Rev. Lett. **77**, 1865 (1996).
[9] Zheng Weihong, V. Kotov, and J. Oitmaa, Phys. Rev. B **57**, 11439 (1998).
[10] D. C. Johnston, M. Troyer, S. Miyahara, D. Lidsky, K. Ueda, M. Azuma, Z. Hiroi, M. Takano, M. Isobe, Y. Ueda, M. A. Korotin, V. I. Anisimov, A. V. Mahajan, and L. L. Miller, cond-mat/0001147 (unpublished).
[11] M. Sigrist and A. Furusaki, J. Phys. Soc. Jpn. **65**, 2385 (1996).
[12] H. Manaka, I. Yamada, and H. Aruga Katori, Phys. Rev. B **63**, 104408 (2001); H. Manaka, I. Yamada, H. Mitamura, and T. Goto, Phys. Rev. B **66**, 064402 (2002).
[13] B. R. Patyal, B. L. Scott, and R. D. Willett, Phys. Rev. B **41**, 1657 (1990); B. C. Watson, V. N. Kotov, M. W. Meisel, D. W. Hall, G. E. Granroth, W. T. Montfrooij, S. E. Nagler, D. A Jensen, R. Backov, M. A. Petruska, G. E. Fanucci, and D. R. Talham, Phys. Rev. Lett. **86**, 5168 (2001).
[14] C. P. Landee, M. M. Turnbull, C. Galeriu, J. Giantsidis, and F. M. Woodward, Phys. Rev. B **63**, 100402(R) (2001).
[15] M. J. Konstantinović, Z. V. Popović, M. Isobe, and Y. Ueda, Phys. Rev. B **61**, 15 185 (2000); T. Ohama, M. Isobe, and Y. Ueda, J. Phys. Soc. Jpn. **70**, 1801 (2001).
[16] R. Mélin, Y.-C. Lin, P. Lajko, H. Rieger, and F. Iglói, Phys. Rev. B **65**, 104415 (2002).
[17] E. Yusuf and K. Yang, Phys. Rev. B **65**, 224428 (2002).
[18] E. Orignac and T. Giamarchi, Phys. Rev. B **57**, 5812 (1998).
[19] M. Steiner, M. Fabrizio, and A. O. Gogolin, Phys. Rev. B **57**, 8290 (1998).
[20] R. A. Hyman, K. Yang, R. N. Bhatt, and S. M. Girvin, Phys. Rev. Lett. **76**, 839 (1996).
[21] A. V. Chubukov, Pis'ma Zh. Eksp. Teor. Fiz. **49**, 108 (1989) [JETP Lett. **49**, 129 (1989)]; A. V. Chubukov and Th. Jolicoeur, Phys. Rev. B **44**, 12050 (1991).
[22] S. Sachdev and R. N. Bhatt, Phys. Rev. B **41**, 9323 (1990).
[23] O. A. Starykh, M. E. Zhitomirsky, D. I. Khomskii, R. R. P. Singh, and K. Ueda, Phys. Rev. Lett. **77**, 2558 (1996).
[24] R. M. White, *Quantum Theory of Magnetism*, McGraw-Hill, New York 1970.
[25] J.-M. vanden Broeck and L. W. Schwartz, Siam. J. Math. Anal. **10**, 658 (1979).
[26] M. Henkel and G. Schütz, J. Phys. A **21**, 2617 (1988).
[27] S. Doniach and E. H. Sondheimer, *Green's Functions for Solid State Physicists*, Imperial College Press, London 1998.
[28] W. Brenig and A. P. Kampf, Phys. Rev. B **43**, 12914 (1991).
[29] R. J. Elliott, J. A. Krumhansl, and P. L. Leath, Rev. Mod. Phys. **46**, 465 (1974).